Computational Fluid Dynamics JOURNAL 14(4):46 January 2006 (pp.401–418)

WAVE INTERACTIONS AND NUMERICAL APPROXIMATION FOR TWO–DIMENSIONAL SCALAR CONSERVATION LAWS

Matania BEN–ARTZI † **Joseph FALCOVITZ** ‡ **Jiequan LI** ♯

Abstract

This paper is concerned with the interplay of the spatial splitting and high resolution schemes for the approximation of solutions to multidimensional scalar conservation laws. We first review the general theory for two–dimensional wave interactions of "Riemann–type". This is followed by a detailed discussion of two cases: The Burgers equation and the Guckenheimer equation. We then utilize the explicit, analytic structure of solutions to test the adaptivity of the one–dimensional Godunov scheme and GRP (Generalized Riemann Problem) scheme to "Strang spatial splitting" and the geometric complexity of the problem. The results demonstrate that both schemes produce a correct approximation to complex 2–D wave–interaction patterns. However, they differ at "fine" points of the solutions, leading to various conclusions concerning the accuracy of numerical schemes.

Key Words: Nonlinear 2–D scalar conservation law, Burgers equation, Guckenheimer equation, Godunov scheme, GRP (Generalized Riemann problem) scheme, Strang operator splitting.

1 Introduction

The purpose of this paper is to explore some aspects encountered in the numerical study of solutions to multi-dimensional scalar conservation laws by high resolution schemes. More precisely, we focus on the interplay between the high resolution schemes, which are basically one-dimensional, and the method of the "spatial splitting", which enables the extension of the 1-D schemes to two-dimensional settings. Our approach here is based on the comparison of the numerical approximation with analytic solutions. Such solutions are obtained in two cases, to be discussed later in detail: The Burgers equation and the Guckenheimer equation. In both cases, the "Riemann–type" problems to be studied are genuinely two–dimensional, leading to non–trivial wave interactions, which nonetheless can be obtained analytically. As pointed out by Lindquist [9,10], "These solutions to two–dimensional Riemann problems also supply a set of problems for testing of finite difference schemes. The richness of structure of these solutions lends itself to this purpose". We note right away that a nonlinear one–dimensional conservation law can be "rotated" in the (x, y) plane, thus forming a "two–dimensional" problem. This, however, cannot lead to the kind of wave interactions discussed here, and will not be considered (even though the consideration of such problems is important in testing the basic features of a numerical scheme).

Received on February 13, 2006.

† Institute of Mathematics, The Hebrew University of Jerusalem; Jerusalem, 91904, Israel; e-mail: mbartzi@math.huji.ac.il

‡ Institute of Mathematics, The Hebrew University of Jerusalem; Jerusalem, 91904, Israel; e-mail: ccjf@math.huji.ac.il

‡ Department of Mathematics, Capital Normal University, Beijing, 100037, P. R. China; e-mail: jiequan@mail.cnu.edu.cn

There are three ingredients in the present work: (a) Analytic solutions involving wave interactions due to the two–dimensional geometry. (b) A high–resolution scheme for one–dimensional conservation laws. (c) A "spatial splitting" technique which enables us to convert the one–dimensional scheme into a two–dimensional one. The point here is to try and study the "mutual interaction" of these ingredients. In particular, while (a)–(b) seem to be well studied, the interaction between (b) and (c) is not yet fully understood (see "Two–dimensional prologue: No dimensional splitting" in [6].

This interaction is influenced by (at least) two factors, namely, the adaptivity of the particular one–dimensional scheme to "spatial splitting" and the geometric complexity of the problem. The latter includes also the interplay between a Cartesian grid and strong curvilinear waves (see [2]).

We consider the initial value problem (IVP) for the equation,

$$u_t + f(u)_x + g(u)_y = 0, \tag{1.1}$$

$$u(x, y, 0) = \phi(x, y), \quad (x, y) \in \mathbb{R}^2, \tag{1.2}$$

where $u(x, y, t)$ is a real (scalar) function and $f(u)$, $g(u)$ are real smooth flux functions.

A "Riemann type" problem for (1.1) is the IVP where $\phi(x, y)$ is finitely valued and homogeneous of order zero,

$$\phi(x, y) = u_0(\theta), \quad \theta = \arg(x, y)(= \arctan \frac{y}{x}), \tag{1.3}$$

and $u_0(\theta)$ is piecewise constant in $[0, 2\pi]$ with finitely many jumps. Recall (see [5]) and the original papers [7,13] that, for any initial function $\phi \in L^\infty(\mathbb{R}^2)$, there exists a unique (weak) solution $u(x, y, t)$ to (1.1)–(1.2). The entropy condition (which includes already the fact that u is indeed a weak solution) can be described as follows.

Let $U(s)$ be a real convex function and $F(s)$ and $G(s)$ functions such that

$$F'(s) = U'(s)f'(s), \quad G'(s) = U'(s)g'(s). \tag{1.4}$$

Then, in the sense of distributions,

$$U(u)_t + F(u)_x + G(u)_y \leq 0. \tag{1.5}$$

The initial value (1.2) is attained in the sense that

$$u(x, y, t) \to \phi(x, y) \quad \text{in } L^1_{loc}(\mathbb{R}^2), \quad \text{as } t \to +0. \tag{1.6}$$

When the initial data is given by (1.3), the uniqueness implies that the solution is "self–similar", namely,

$$u(x, y, t) = u(x/t, y/t, 1), \quad t > 0. \tag{1.7}$$

In what follows we shall use the similarity coordinates

$$\xi = \frac{x}{t}, \quad \eta = \frac{y}{t}, \tag{1.8}$$

and set $v(\xi, \eta) = u(\xi, \eta, 1)$.

The solutions to the Riemann–type problem (1.1)–(1.3) display a rich variety of wave patterns, some of which are far from being "evident". We refer to [4,8,14,15,16] for a thorough presentation. Our intention in this paper is to show that this variety can serve as a basis for the investigation of "fine points and subtleties" pertinent to high resolution schemes. Unlike the "one–dimensional test cases" (most of which have been carried out only for the Burgers equation), the truly two–dimensional wave structures, combined with the inherent "spatial splitting" of the numerical schemes, poses a considerable challenge. We remark that the description of geometric shapes in Cartesian grids presents already a nontrivial difficulty for the schemes (see [2])

The structure of this paper is as follows. In Section 2 we review the basic theory concerning the IVP (1.1)–(1.2). In Section 3, we discuss in detail the solutions for two cases of fluxes. The first is the Burgers equation $f(u) = g(u) = \frac{1}{2}u^2$, where we consider four examples. Even in this rather elementary case, we demonstrate various possibilities of wave interactions. Next we describe the solution for the "Guckenheimer equation", where $f(u) = \frac{1}{2}u^2$ and $g(u) = \frac{1}{3}u^3$. In Section 4, we recall the details of our high resolution approach, based on the GRP (Generalized Riemann Problem) scheme. The two–dimensional numerical simulation is carried out using a "spatial splitting" technique. In Section 5, we give numerical results both for the Godunov (first order) scheme and GRP scheme and discuss their differences.

2 The Analysis of 2–D Riemann–Type Solutions

We recall here the basic facts concerning solutions of (1.1)–(1.3). Using the similarity notation (1.7)–(1.8), we refer to the solution as $v(\xi, \eta)$. Note that the initial condition (1.3) now becomes

$$u_0(\theta) = \lim_{r\to\infty} v(r\cos\theta, r\sin\theta), \quad 0 \le \theta \le 2\pi. \tag{2.1}$$

In general terms, the IVP can be cast in terms of an equation for v (in the (ξ, η) plane) with a boundary condition (2.1) imposed at the "circle at infinity". In fact, due to finite propagation speed, the solution consists of separate 1–D waves (emanating from rays in direction of the jumps of $u_0(\theta)$). These waves interact in a disk centered at the origin, and the difficulty lies in the need to account for the interactions, subject to the entropy conditions.

In regions of smooth solution (i.e., where $v(\xi, \eta) \in C^1$), we have from (1.1),

$$(-\xi + f'(v))v_\xi + (-\eta + g'(v))v_\eta = 0, \tag{2.2}$$

which is a quasilinear equation. Its characteristic curves carry constant values of v, and are therefore straight lines (terminating at singularities). Let L_C be the line carrying the value $v = C$. By (2.2) it is an integral line for the field $\Phi_C(\xi, \eta) = (-\xi + f'(C), -\eta + g'(C))$, hence lies on a ray emanating from the critical point $z_C := (f'(C), g'(C))$. We orient it, by convention, in the direction of z_C.

Remark 2.1. *Note that by (1.1), the characteristic lines L_C are just the traces of the bicharacteristic lines for (1.1) on the (x, y)–plane, now identified as the (ξ, η) plane. The chosen orientation for L_C (towards z_C) corresponds to orienting the bicharacteristic line in the direction $t \to +\infty$ (so that $(\xi, \eta) = (\frac{x}{t}, \frac{y}{t})$ approaches z_C).*

Definition 2.2. *The "critical set" $\Gamma(v)$ for Eq. (2.2) is the set of all possible points z_C, i.e.,*

$$\Gamma(v) = \{(f'(C), g'(C)), C = v(z_C), \textit{for some } z_C \in \mathbb{R}^2\}. \tag{2.3}$$

We now turn to conditions imposed on jump discontinuities of solutions to (2.2). Using the standard procedure for the definition of weak solutions, we obtain the Rankine–Hugoniot jump relations.

Claim 2.3. *Let $\eta = \eta(\xi)$ be the (C^1) trajectory of a jump discontinuity. Then the slope $\sigma = \eta'(\xi)$ satisfies the R–H condition*

$$\sigma = \frac{\eta - g'_{+,-}}{\xi - f'_{+,-}}, \tag{2.4}$$

where $h'_{+,-} = \frac{h(v_+)-h(v_-)}{v_+-v_-}$ and $v_\pm$ are the limiting values of the solution v at the jump.

Proof 2.4. *Note that by the standard procedure (see [5])applied to (2.2) in the form*

$$(-\xi v + f(v))_\xi + (-\eta v + g(v))_\eta + 2v = 0, \tag{2.5}$$

we get

$$\sigma = \frac{-\eta(v_+ - v_-) + g(v_+) - g(v_-)}{-\xi(v_+ - v_-) + f(v_+) - f(v_-)},$$

which reduces to (2.4).

Remark 2.5. *As in the case of Remark 2.1, the R–H condition (2.4) can be derived by applying the notion of a weak solution directly to Eq. (1.1). In this case, a surface of discontinuity in the (x, y, t) variables is expressed in a self–similar form $y = t\eta(\frac{x}{t})$, and the R–H condition is applied to the normal direction $(\sigma, -1, \eta - \xi\sigma)$, where $\sigma = \eta'(\xi)$ (and $(\xi, \eta) = (\frac{x}{t}, \frac{y}{t})$). In particular, the "effective" flux function in this direction (see [5]) is*

$$H_\sigma(v) = \sigma f(v) - g(v). \tag{2.6}$$

The entropy (admissibility) condition on jump discontinuities is most easily obtained by resorting to the (x, y, t) setting and the "directional" flux H_σ, as in (2.6). Using the convention $v_- < v_+$, we get [11]

$$\frac{H_\sigma(k) - H_\sigma(v_-)}{k - v_-} \geq \frac{H_\sigma(v_+) - H_\sigma(v_-)}{v_+ - v_-}, \quad k \in [v_-, v_+] \tag{2.7}$$

as a necessary and sufficient condition for a jump (v_-, v_+) whose slope is $\sigma = \eta'(\xi)$.

In analogy with $\Gamma(v)$ (see(2.3)), we define the set (for a given solution v and a fixed state $\overline{v}$),

$$\Gamma_s(v; \overline{v}) = \{(f'_{+,-}, g'_{+,-}), v_- = \overline{v}, v_+ = v(\xi_+, \eta_+) \text{ for some } (\xi_+, \eta_+) \in \mathbb{R}^2\}. \tag{2.8}$$

We consider $\Gamma_s(v; \overline{v})$ as a subset of the (ξ, η) plane. In view of (2.4), it has the following geometric interpretation. If l is a tangent line to a smooth discontinuity curve, and v takes on the value $\overline{v}$ at the tangency point (on either side) then l intersects $\Gamma_s(v; \overline{v})$.

The entropy condition (2.7) implies, as is well–known, that all bicharacteristic lines (in (x, y, t)) "impinge" on the shock surface, as $t \to +\infty$ (or are tangent to it). In view of Remark 2.1 and our convention for the orientation of characteristic curve in the (ξ, η) plane, we obtain the following corollary.

Corollary 2.6. *If $\eta = \eta(\xi)$ is the trajectory of an admissible shock, then the characteristic lines on its two sides run "into it" (with the given orientation) or are tangent to it (so that the shock becomes sonic on that side).*

The structure of a centered rarefaction wave (CRW) in the (ξ, η) plane is derived from the discussion of characteristic lines and their directions. For clarity we state it in the following claim.

Claim 2.7. *A CRW centered at (ξ_0, η_0) is given by the sector*

$$\alpha \le \frac{\eta - \eta_0}{\xi - \xi_0} \le \beta,$$

where, for any direction $r \in [\alpha, \beta]$, $v = C_r$ such that

$$r = \frac{g'(C_r) - \eta_0}{f'(C_r) - \xi_0}. \tag{2.9}$$

Remark 2.8. *Observe that this CRW corresponds to a rather complex structure in the original (x, y, t) setting; the vertex (ξ_0, η_0) represents the line $x = \xi_0 t$, $y = \eta_0 t$. At every time level t there is a (rarefaction) fan of rays emanating from (x, y, t) and carrying constant values of u. The whole structure moves in a self–similar fashion as t grows. The rays then become planes (carrying constant values of u) whose traces on the (ξ, η) plane satisfy (2.9).*

We can summarize the procedure for the solution of the Riemann–type problem (1.1)–(1.3) as follows.

(a) The problem is restated as Eq. (2.2) in the (ξ, η) plane, where the function $v(\xi, \eta)$ satisfies the boundary condition (2.1).

(b) Outside of a sufficiently large disk (in (ξ, η)) we determine the 1–D waves issuing at the jump discontinuities of $u_0(\theta)$ in the (x, y, t) setting, and determine $v(\xi, \eta) = u(\xi, \eta, 1)$.

(c) The resulting waves are extended into the disk, where they interact and produce additional waves (CRW or shocks), subject to the conditions (2.7) (shocks) and (2.9) (CRW).

As we shall see in the following examples, this last step can be quite involved, producing surprising structures. For general treatments, we refer to [4,8,15].

3 Two Examples of Riemann–Type Solutions

3.1 The Burgers (2–D) Equation, $f(u) = g(u) = \frac{1}{2}u^2$.

Here the two singular sets $\Gamma(v)$, $\Gamma_s(v; \overline{v})$ (see (2.3), (2.8)) are easily seen to be identical (and independent of $\overline{v}$ for $\Gamma_s(v, \overline{v})$),

$$\Gamma(v), \quad \Gamma_s(v; \overline{v}) \subseteq \{(\xi, \eta) \in \mathbb{R}^2, \xi = \eta\}.$$

We refer to [9,1.,14] for the study of the equation with four constant values in the four quadrants.

(i) As a first case, take the initial data

$$u_0(\theta) = \begin{cases} 1, & 0 < \theta < \frac{\pi}{2}, \\ -1, & \text{otherwise.} \end{cases} \tag{3.1}$$

If we think in terms of the original problem (1.1)–(1.3), it means that $u(x,y,0) = 1$ in the first quadrant and -1 otherwise. Outside of a large disk, we obtain two noninteracting rarefaction waves, emanating from $\{x > 0, y = 0\}$ and $\{x = 0, y > 0\}$. The solution at $t = 1$ is therefore given by (with $\xi = x$, $\eta = y$),

$$u(x,y,1) = v(\xi,\eta) = \begin{cases} 1, & \xi > 1 \text{ and } \eta > 1, \\ -1, & \xi < -1 \text{ or } \eta < -1, \\ \eta, & \xi > \eta \text{ and } -1 < \eta < 1, \\ \xi, & \eta > \xi \text{ and } -1 < \xi < 1, \end{cases} \tag{3.2}$$

(see Figure 3.1(a)).

Note that since the waves do not interact, we could extend them to the full (ξ,η) plane. (ii) Reversing the initial data (3.1), we now study the Burgers equation with

$$u_0(\theta) = \begin{cases} -1, & 0 < \theta < \frac{\pi}{2}, \\ 1, & \text{otherwise.} \end{cases} \tag{3.3}$$

Turning once again to the original problem (1.1)–(1.3), the solution at $t = 1$, outside of a large disk, consists of standing shocks along $y = 0$ (and $x > 0$) and $x = 0$ ($y > 0$). It can be checked that they extend to the origin without interacting (and satisfy the entropy condition), so that the solution now is

$$v(\xi,\eta) = \begin{cases} -1, & \xi > 0, \eta > 0, \\ 1, & \text{otherwise,} \end{cases} \tag{3.4}$$

(see Figure 3.1(b)).

(iii) Now we take the initial data

$$u_0(\theta) = \begin{cases} -1, & 0 < \theta < \frac{\pi}{2}, \\ 1 & \frac{\pi}{2} < \theta < \theta_0, \\ 0, & \theta_0 < \theta < 2\pi, \end{cases} \tag{3.5}$$

where $\pi < \theta_0 < \frac{3\pi}{2}$ satisfies $\tan\theta_0 = 2$ (so that the jump between 1 and 0 lies along $y = 2x$, $x < 0$). Thus, at time $t > 0$, outside of a large disk we have three shocks (in the (x,y) plane):

(a) A shock along $y = -\frac{1}{2}t$ moving at speed $-\frac{1}{2}$ (in the y–direction).

(b) A standing shock along $x = 0$, $y > 0$.

(c) A shock at $2x - y = \frac{1}{2}t$ (for x sufficiently negative). This shock can easily be determined from (2.4) if we note that $\sigma = 2$ and $f'_{+,-} = g'_{+,-} = \dfrac{1}{2}$ (for $v_+ = 1$, $v_- = 0$).

It is easily seen that all shocks (a)–(c) satisfy the entropy conditions (since all characteristics are directed towards $\xi = \eta$ and thus "incoming"). Note that by (2.8) (and the paragraph following it) the shock (b) is directed towards $(0,0) \in \Gamma_s(-1;1)$ and can only be extended to that point. The shocks

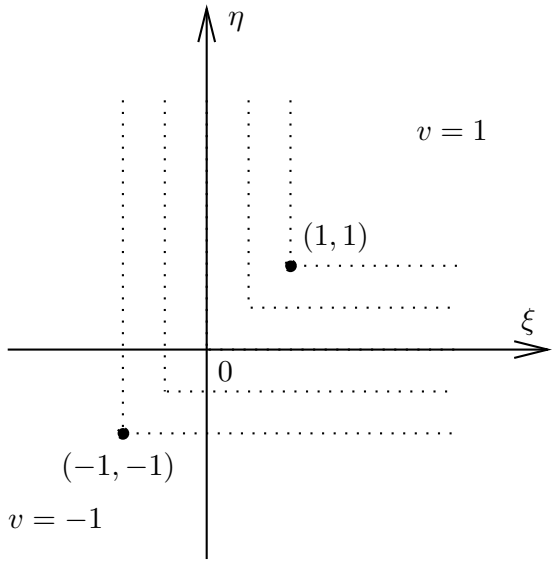

(a) Solution for Case (i)

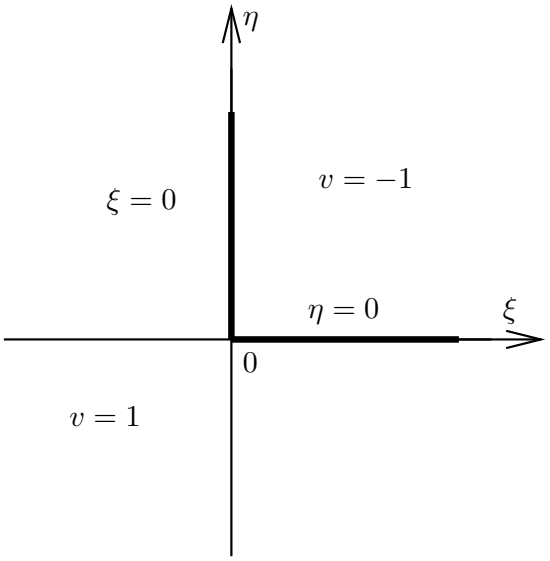

(b) Solution for Case (ii)

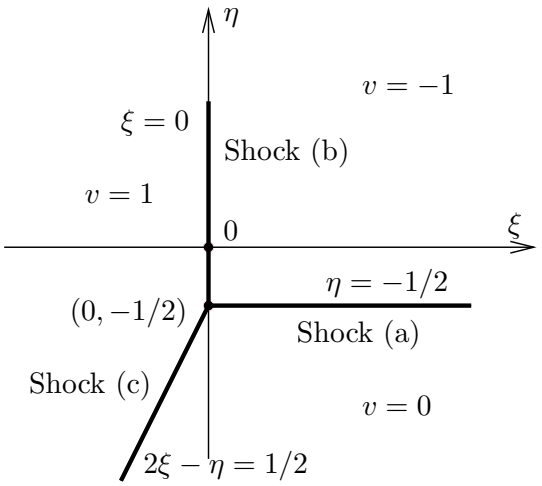

(c) Solution for Case (iii)

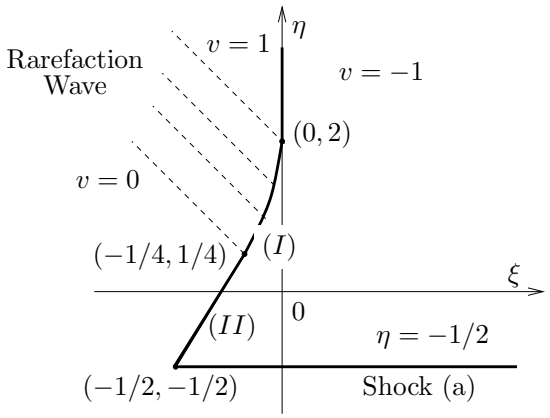

(d) Solution for Case (iv)

Fig.3.1: Full solutions of the Burgers equation for cases (i)–(iv) 3.1

(a) and (c) interact at $(0, -\frac{1}{2})$, where we solve the Riemann problem for (2.2) locally with the data 1 and -1 on two sides to get the additional shock segment $\xi = 0$, $-\dfrac{1}{2} \le \eta \le 0$. The full solution is shown in Figure 3.1 (c).

(iv) Finally, we take the initial data,

$$u_0(\theta) = \begin{cases} -1, & 0 < \theta < \dfrac{\pi}{2}, \\ 1, & \dfrac{\pi}{2} < \theta < \dfrac{3\pi}{4}, \\ 0 & \dfrac{3\pi}{4} < \theta < 2\pi. \end{cases} \tag{3.6}$$

As before we start by looking at the solution in the (x, y, t) frame, outside of a large disk. Clearly, as in the previous case, we have the two shocks (a), (b) (see Figure 3.1 (c)). However, instead of the third shock we have now a rarefaction wave which propagates parallel to the line $x+y=0$ (as in Case (i)). Turning to the (ξ, η) plane, the solution is as shown in Figure 3.1 (d).

The characteristic line $\xi + \eta = k$, $k \geq 0$, intersects the set Γ at $(\frac{k}{2}, \frac{k}{2})$, and thus, by (2.3), carries the value $v = \frac{k}{2} = \frac{\xi+\eta}{2}$. Since $v = 1$ at the leading characteristic, we have there $k = 2$, and this characteristic intersects the standing shock at $\eta = 2$. Below this point, the standing shock interacts with the rarefaction wave and decreases in strength. It is therefore diverted into the region $\xi < 0$. Let (I) be the shock between (0,2) and the tail characteristic $\xi + \eta = 0$ (see Figure 3.1 (d)), expressed as $\eta = \eta(\xi)$. For $\sigma = \eta'(\xi)$, we have by (2.4), since $v_+(\xi, \eta) = \frac{1}{2}(\xi + \eta)$, $v_- = -1$,

$$\eta'(\xi) = \frac{\eta - \frac{1}{2} \cdot \frac{v_+^2 - v_-^2}{v_+ - v_-}}{\xi - \frac{1}{2} \cdot \frac{v_+^2 - v_-^2}{v_+ - v_-}} = \frac{\eta - \frac{1}{2} \cdot (\frac{\xi+\eta}{2} - 1)}{\xi - \frac{1}{2} \cdot (\frac{\xi+\eta}{2} - 1)},$$

and since $\eta'(\xi) = +\infty$ as $\xi \to 0$, we use the inverse function to write,

$$\xi'(\eta) = \frac{-\xi + 3\eta + 2}{3\xi - \eta + 2}, \quad \xi'(2) = 0. \tag{3.7}$$

The solution of this equation is given by $(\xi + \eta + 2)^2 + 8(\xi - \eta) = 0$. Thus the shock (I) intersects the line $\xi + \eta = 0$ at $(-\frac{1}{4}, \frac{1}{4})$. The next interesting feature of the solution is the existence of the shock (II) connecting $(-\frac{1}{4}, \frac{1}{4})$ to $(-\frac{1}{2}, -\frac{1}{2})$. It is a straight line having slope 3 by (2.4). This shock represents an additional phenomenon, namely, the interaction of the shocks (a) and (b) (or its part (I)). This phenomenon is very common in the case of systems, but has no analog in the case of a single scalar conservation law in one space dimension.

Remark 3.1. *Consider the one–dimensional Burgers equation $u_t + (\frac{1}{2}u^2)_x = 0$, subject to the initial data*

$$u_0(x) = \begin{cases} 0, & x < 0 \text{ or } x > 1, \\ 1, & 0 < x < 1. \end{cases}$$

The solution now consists of a centered rarefaction fan emanating from $(0, 0)$ and taking over the shock emanating from $(1, 0)$ (see Figs.3 and 4). Gradually, the rarefaction " consumes" the shock and $\max_{x\in\mathbb{R}} u(x, t)$ tends to 0 as $t \to +\infty$. However, this is an interaction in time, whereas, the interaction leading to the formation of the shock (II) in Figure 3.1 (d) is spatial. The latter can be viewed as analog to the formation of Mach Stems in the 2–D fluid dynamical setting.

3.2 The Guckenheimer Equation, $f(u) = \frac{1}{2}u^2$, $g(u) = \frac{1}{3}u^3$.

This equation was first studied by Guckenheimer in [4]. Here we take the initial data

$$u_0(\theta) = \begin{cases} 0, & 0 < \theta < \frac{3\pi}{4}, \\ 1, & \frac{3\pi}{4} < \theta < \frac{3\pi}{2}, \\ -1, & \frac{3\pi}{2} < \pi < 2\pi. \end{cases} \tag{3.8}$$

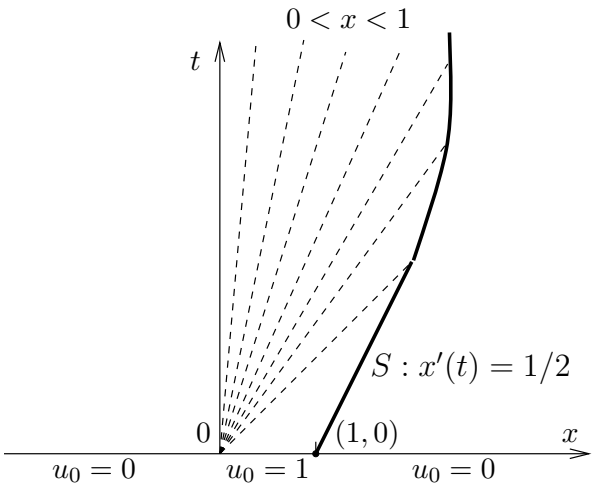

Fig.3.2: Wave interaction for the one-dimensional Burgers equation.

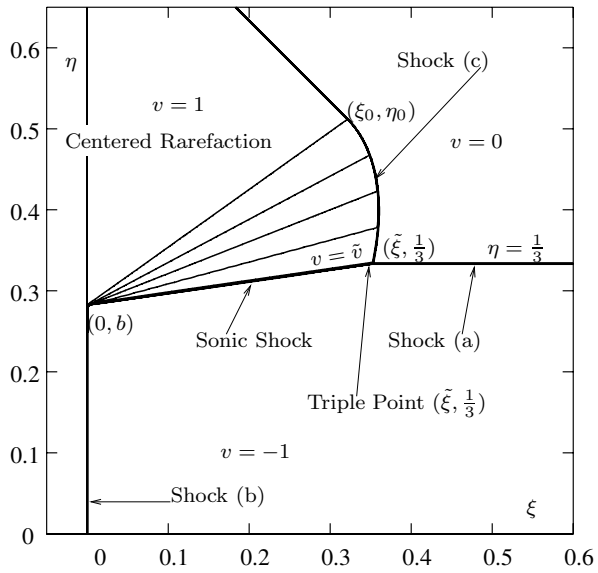

Fig.3.3: Guckenheimer structure

Outside of a large disk we obtain three shocks (see Figure 3.1):

(a) A shock emanating from $y = 0$ and moving at speed $\frac{1}{3}$ in the positive y direction (note that u^3 is concave on $[-1, 0]$). In the (ξ, η) plane it is given by $\eta = \frac{1}{3}$.

(b) A standing shock along $\xi = 0$ $(\eta < 0)$.

(c) A shock emanating from the line $x + y = 0$. In the (ξ, η) plane we note that, in view of (2.4), (2.8), it is directed towards $(\frac{1}{2}, \frac{1}{3})$ and is therefore given by $\xi + \eta = \frac{5}{6}$.

The interaction of these three shocks in a disk around $(0, 0)$ form a very complex wave structure (see [4,15,8] for details), which can be described as follows (see Figure 3.1), in the (ξ, η) plane.

At a certain point $(0, b)$, $0 < b < \frac{1}{3}$, the shock (b) bifurcates into a centered rarefaction wave (CRW) whose leading characteristic is a sonic shock, across which the solution v jumps from -1 to a (still unknown) value $\widetilde{v}$. Then v increases across the rarefaction from $\widetilde{v}$ to 1. The rarefaction wave modifies shock (c) in a fashion similar to that of the part (I) of the shock in the previous example of the Burgers equation (Case (iv)). Note that the tail characteristic of the CRW carries the value $v = 1$, hence by (2.3) is directed towards $(1, 1)$. It intersects the shock (c) at a point (ξ_0, η_0) such that

$$\xi_0 + \eta_0 = \frac{5}{6}, \quad \frac{\eta_0 - b}{\xi_0} = 1 - b,$$

hence

$$\xi_0 = \frac{\frac{5}{6} - b}{2 - b}, \quad \eta_0 = \frac{\frac{5}{6} + \frac{1}{6}b}{2 - b}. \tag{3.9}$$

The leading characteristic (sonic shock) carries the value $\widetilde{v}$ (which we should use when viewing it as a characteristic line) and is therefore directed towards $(\widetilde{v}, \widetilde{v}^2)$. It intersects the shock (a) at $(\widetilde{\xi}, \frac{1}{3})$, where

$$\frac{\frac{1}{3} - b}{\widetilde{\xi}} = \frac{\widetilde{v}^2 - b}{\widetilde{v}}$$

so that

$$\widetilde{\xi} = \frac{(\frac{1}{3} - b)\widetilde{v}}{\widetilde{v}^{\,2} - b}. \tag{3.10}$$

From the shock relation (2.4) across the sonic shock we obtain a relation between $\widetilde{v}$, b as follows,

$$\frac{\frac{1}{3} - b}{\widetilde{\xi}} = \frac{\frac{1}{3} - \frac{1}{3}(\frac{\widetilde{v}^{\,3}+1}{\widetilde{v}+1})}{\widetilde{\xi} - \frac{1}{2}(\frac{\widetilde{v}^{\,2}-1}{\widetilde{v}+1})} = \frac{\frac{1}{3} - \frac{1}{3}\cdot(\widetilde{v}^{\,2} - \widetilde{v} + 1)}{\widetilde{\xi} - \frac{1}{2}\cdot(\widetilde{v} - 1)}, \tag{3.11}$$

where $\widetilde{\xi}$ is expressed in terms of b, $\widetilde{v}$ by (3.10). We get,

$$\frac{\widetilde{v}^{\,2} - b}{\widetilde{v}} = \frac{\frac{1}{3}\cdot\widetilde{v}\,(1 - \widetilde{v}\,)}{\frac{(1/3-b)\widetilde{v}}{\widetilde{v}^{\,2}-b} - \frac{1}{2}(\widetilde{v} - 1)},$$

namely,

$$b = \frac{1}{3} + \frac{(1 - \widetilde{v}\,)(\frac{1}{3}\widetilde{v}^{\,2} - \frac{1}{2})}{\widetilde{v}}. \tag{3.12}$$

Thus, $\widetilde{v}$ remains as the only parameter to be determined.

The result of the interaction between the CRW and the shock (c) leads, as noted above, to a "bending" of the latter, forming a shock branch $\eta = \eta(\xi)$ between (ξ_0, η_0) and $(\widetilde{\xi}, \frac{1}{3})$. Let L_C be the characteristic line in the CRW, carrying the value $v \equiv C$, $C \in [\widetilde{v}, 1]$. If it intersects the shock branch at ξ_C, $\eta_C = \eta(\xi_C)$, we have by (2.4) (with $v_+ = C$, $v_- = 0$),

$$\eta'(\xi_C) = \frac{\eta_C - \frac{1}{3}C^2}{\xi_C - \frac{1}{2}C}. \tag{3.13}$$

However, since L_C is directed towards (C, C^2), we have also,

$$\frac{\eta_C - b}{\xi_C} = \frac{C^2 - b}{C},$$

hence (since $\widetilde{v} > 0$),

$$C = C(\xi_C, \eta_C) = \frac{\eta_C - b + \sqrt{(\eta_C - b)^2 + 4b\xi_C^2}}{2\xi_C}. \tag{3.14}$$

Inserting (3.14) in (3.13) and suppressing the subscript "C", we obtain an ordinary differetial equation for the shock branch $\eta = \eta(\xi)$,

$$\eta'(\xi) = \frac{\eta(\xi) - \frac{1}{3}C(\xi, \eta(\xi))^2}{\xi - \frac{1}{2}C(\xi, \eta(\xi))}. \tag{3.15}$$

The equation depends on the parameter $\widetilde{v}$, and its solution should connect (ξ_0, η_0) to $(\widetilde{\xi}, \frac{1}{3})$.

Choosing a value $b \in (0, 1/3)$, ξ_0, η_0 are determined by (3.9), $\widetilde{v}$ by (3.12) and $\widetilde{\xi}$ by (3.10). Also the function $C(\xi, \eta)$ is determined by (3.14). The differential equation (3.15) is then solved (using in practice a fourth order Range–Kutta method), starting at (ξ_0, η_0). The solution $\eta(\xi)$ then intersects the line $\eta = \frac{1}{3}$ at $\xi = \xi_b$. We modify b (by a shooting method) until we get $\xi_b = \widetilde{\xi}$.

For our case here the values obtained are

$$b = 0.282305677, \quad \widetilde{v} = 0.608741813, \quad \widetilde{\xi} = 0.35196101.$$

4 The numerical method associated with GRP scheme

In this section we recall our high resolution approach to approximate ([4]) by using a "Strang–type" operator splitting to divide Eq. (1.1) into two simpler one–dimensional conservation laws (see [12]),

$$u_t + f(u)_x = 0, \tag{4.1}$$

$$u_t + g(u)_y = 0. \tag{4.2}$$

Then we implement the GRP (Generalized Riemann Problem) scheme [1] to each of these two equations.

We begin with the GRP scheme for (4.1). Take an equally spaced grid in $\mathbb{R}$, $x_{j+\frac{1}{2}} = (j+\frac{1}{2})h$, $j \in \mathbb{Z}$. At each time level t_n, it is assumed that the solution $u(x,t_n)$ is approximated by a piecewise linear function.

$$w^n(x) = w_j^n + (x - x_j)s_j^n, \qquad x \in (x_{j-\frac{1}{2}}, x_{j+\frac{1}{2}}), \tag{4.3}$$

and the value w_j^n is the average of $w^n(x)$ in "cell j" $(=(x_{j-\frac{1}{2}}, x_{j+\frac{1}{2}}))$ and is associated with its center $x_j = \frac{1}{2}(x_{j-\frac{1}{2}} + x_{j+\frac{1}{2}})$, and s_j^n is the slope of $w^n(x)$ in cell j. Let $U(x,t)$ be the exact solution of (4.1) with the initial data $U(x,t_n) = w^n(x)$. Then the approximate averages w_j^{n+1} are determined by

$$w_j^{n+1} = w_j^n - \lambda(f_{j+\frac{1}{2}}^{n+\frac{1}{2}} - f_{j-\frac{1}{2}}^{n+\frac{1}{2}}), \tag{4.4}$$

where $\lambda = \frac{k}{h}$ and the numerical flux $f_{j+\frac{1}{2}}^{n+\frac{1}{2}}$ should approximate the time average of $f(U(x_{j+\frac{1}{2}}, t))$, $t_n \le t \le t_{n+1} = t_n + k$.

In the first step, we evaluate $w_{j+\frac{1}{2}}^n$ by

$$w_{j+\frac{1}{2}}^n = R(0; w_{j+\frac{1}{2},\mp}^n), \tag{4.5}$$

where $R(\frac{x}{t}; \alpha_\mp)$ is the (self–similar) solution to the Riemann problem for (4.1), having initial data $\alpha_\mp$ as $\mp x > 0$. The limiting values $w_{j+\frac{1}{2},\mp}^n$ appearing in (4.5) are defined by

$$w_{j+\frac{1}{2},\mp}^n = \lim_{x \to x_{j+\frac{1}{2}}\mp} w^n(x). \tag{4.6}$$

Thus, the value $w_{j+\frac{1}{2}}^n$ is the "instantaneous" value obtained by solving the Riemann problem with the limiting values of $w^n(x)$ at the cell boundary $x_{j+\frac{1}{2}}$. The Riemann solution is determined simply as follows.

(i) $w_{j+\frac{1}{2}}^n = z$ such that $f(z) = \min\{f(w); w \in [w_{j+\frac{1}{2},-}^n, w_{j+\frac{1}{2},+}^n]\}$ if $w_{j+\frac{1}{2},-}^n \le w_{j+\frac{1}{2},+}^n$, or,

(ii) $w_{j+\frac{1}{2}}^n = z$ such that $f(z) = \max\{f(w); w \in [w_{j+\frac{1}{2},+}^n, w_{j+\frac{1}{2},-}^n]\}$ if $w_{j+\frac{1}{2},+}^n \le w_{j+\frac{1}{2},-}^n$.

In the Godunov scheme, we always take $s_j^n = s_{j+1}^n = 0$ and set $w_{j+\frac{1}{2}}^{n+\frac{1}{2}} = w_{j+\frac{1}{2}}^n$ ([3]). We note that the wave moves to the right (resp. the left) if $f'(w_{j+\frac{1}{2}}^n) > 0$ (resp. $f'(w_{j+\frac{1}{2}}^n) < 0$). If $w_{j+\frac{1}{2}}^n \ne w_{j+\frac{1}{2},\pm}^n$, then the point is sonic and $f'(w_{j+\frac{1}{2}}^n) = 0$.

The crucial ingredient in the GRP method is the assumption that both $U(x_{j+\frac{1}{2}},t)$ *and* $f(U(x_{j+\frac{1}{2}},t))$ *are approximated linearly (in* $t\in[t_n,t_{n+1}]$*).* We obtain the linear expressions,

$$\widetilde{u}\,(x_{j+\frac{1}{2}},t)=w^n_{j+\frac{1}{2}}+\left(\frac{\partial U}{\partial t}\right)^n_{j+\frac{1}{2}}(t-t_n), \tag{4.7}$$

$$\widetilde{f}\,(\widetilde{u}\,(x_{j+\frac{1}{2}},t))=f(w^n_{j+\frac{1}{2}})+f'(w^n_{j+\frac{1}{2}})\left(\frac{\partial U}{\partial t}\right)^n_{j+\frac{1}{2}}(t-t_n). \tag{4.8}$$

The exact instantaneous value of $\left(\frac{\partial U}{\partial t}\right)^n_{j+\frac{1}{2}}$ at the cell boundary is obtained from (4.1),

$$\left(\frac{\partial U}{\partial t}\right)^n_{j+\frac{1}{2}}=\begin{cases}-f'(w^n_{j+\frac{1}{2}})s^n_j, & \text{if the wave moves to the right,}\\ -f'(w^n_{j+\frac{1}{2}})s^n_{j+1}, & \text{if the wave moves to the left,}\\ 0, & \text{if } x_{j+\frac{1}{2}} \text{ is a sonic point.}\end{cases} \tag{4.9}$$

Then, as the second step, we define the GRP fluxes in (4.4) by

$$w^{n+\frac{1}{2}}_{j+\frac{1}{2}}=\widetilde{u}\,(x_{j+\frac{1}{2}},t_n+\frac{\Delta t}{2}), \tag{4.10}$$

$$f^{n+\frac{1}{2}}_{j+\frac{1}{2}}=\widetilde{f}\,(w^{n+\frac{1}{2}}_{j+\frac{1}{2}}),\qquad -\infty<j<\infty. \tag{4.11}$$

Thus w^{n+1}_j is determined by (4.4).

Remark 4.1. *(Stationary shocks). If the Riemann solution* $R(\frac{x-x_{j+\frac{1}{2}}}{t-t_n};w^n_{j+\frac{1}{2},\pm})$ *yields a stationary shock along* $x=x_{j+\frac{1}{2}}$ *we note that* $f(w^n_{j+\frac{1}{2},-})=f(w^n_{j+\frac{1}{2},+})$, $w^n_{j+\frac{1}{2},-}>w^n_{j+\frac{1}{2},+}$, *so that the shock speed*

$$s(t)=\frac{f(U^+(x_{j+\frac{1}{2}},t))-f(U^-(x_{j+\frac{1}{2}},t))}{U^+(x_{j+\frac{1}{2}},t))-U^-(x_{j+\frac{1}{2}},t)} \tag{4.12}$$

($U^\pm(x_{j+\frac{1}{2}},t)$ *are the values of* U *on the two sides of the shock,* $U^\pm(x_{j+\frac{1}{2}},t_n)=w^n_{j+\frac{1}{2},\pm}$*) can be differentiated to yield,*

$$s'(t)|_{t=t_n}=\frac{-f'(w^n_{j+\frac{1}{2},+})^2s^n_{j+1}+f'(w^n_{j+\frac{1}{2},-})^2s^n_j}{w^n_{j+\frac{1}{2},+}-w^n_{j+\frac{1}{2},-}}. \tag{4.13}$$

The value of $\left(\frac{\partial U}{\partial t}\right)^n_{j+\frac{1}{2}}$ *in (4.9) is determined according to whether* $\pm s'(t_n)>0$ *and* $w^n_{j+\frac{1}{2}}$ *is replaced by one of the values of* $w^n_{j+\frac{1}{2},\pm}$*, taken from the "smooth side".*

Now we need to update $w^{n+1}(x)$ in (4.3), i.e., the new slopes s^{n+1}_j are calculated in two steps.

Step 1. Determine $w_{j+\frac{1}{2}}^{n+1} = \widetilde{u}\,(x_{j+\frac{1}{2}}, t_{n+1})$ by (4.7) and then set

$$\widetilde{s}_j^{n+1} = \frac{1}{\Delta x}(w_{j+\frac{1}{2}}^{n+1} - w_{j-\frac{1}{2}}^{n+1}). \tag{4.14}$$

Step 2 (" Limiter Algorithm"). Set the final value for some $\theta \in (0, 2]$,

$$s_j^{n+1} = \frac{1}{\Delta x}\text{minmod}((2-\theta)(w_{j+1}^{n+1} - w_j^{n+1}), \Delta x \widetilde{s}_j^{n+1}, (2-\theta)(w_j^{n+1} - w_{j-1}^{n+1})), \tag{4.15}$$

where the minmod function is defined by,

$$\text{minmod}(a,b,c) = \begin{cases} s\min(|a|,|b|,|c|), & \text{if } s = \text{sign}(a) = \text{sign}(b) = \text{sign}(c), \\ 0, & \text{otherwise,} \end{cases} \tag{4.16}$$

In practice, we adopt $\theta = 0$.

Next, we apply a "Strang–type" operator splitting to (1.1). Let $S(\Delta t)$, $S_x(\Delta t)$ and $S_y(\Delta t)$ be difference approximation operators for integration by a time step Δt of (1.1), (4.1) and (4.2), respectively. Here the one dimensional operator $S_x(\Delta t)$ (resp. $S_y(\Delta t)$) is given by our GRP scheme described above. Then the Strang–type operator sequence reads

$$S(\Delta t) = S_x(\frac{1}{2}\Delta t)S_y(\Delta t)S_x(\frac{1}{2}\Delta t), \tag{4.17}$$

which means that the evaluation of an initial data $\widetilde{u}$ by (1.1) over a short time Δt is approximated by first evolving $\widetilde{u}$ subject to (4.1) over time $\frac{1}{2}\Delta t$ to obtain u_1, then evolving u_1 in accordance with (4.2) over time Δt to get u_2 and evolving u_2 again over time $\frac{1}{2}\Delta t$ subject to (4.1). This is a second order finite difference approximation to (1.1), as shown in [12].

To secure the numerical stability, we require that the CFL condition holds separately with respect to each of the split one–dimensional equations (4.1), (4.2). The resulting average values in cells are now denoted by $w_{i,j}^n$. Thus, the CFL condition for (1.1) becomes

$$\nu = \max\{|f'(w_{i,j}^n)|\frac{k}{\Delta x}, |g'(w_{i,j}^n)|\frac{k}{\Delta y}\} < 1. \tag{4.18}$$

In our computation (see Section 5), the CFL condition is computed according to (4.18) at each time level, the maximum value over all time levels is retained. Indeed, the CFL condition for (1.1) is readily determined because the maximum value of solutions is controlled by the initial data.

5 Numerical examples

In this section we present numerical results for the problems of Section 3, using our GRP high resolution approach. Our numerical solutions are all given both by the Godunov schemes and the GRP scheme with CFL condition $\nu \leq 0.5$. The computations for the Burgers equation are carried out in the domain $[-1.5, 1.5]$ which is divided into 300×300 uniform cells and are illustrated by contour curves at the final time $T = 1$. We display the results of all four cases for this equation. We refer to [6, Section 4] for a numerical computation of a solution to a two–dimensional Burgers equation. In their case, however, no analytic solution is available. We then proceed to present numerical results for the Guckenheimer equation.

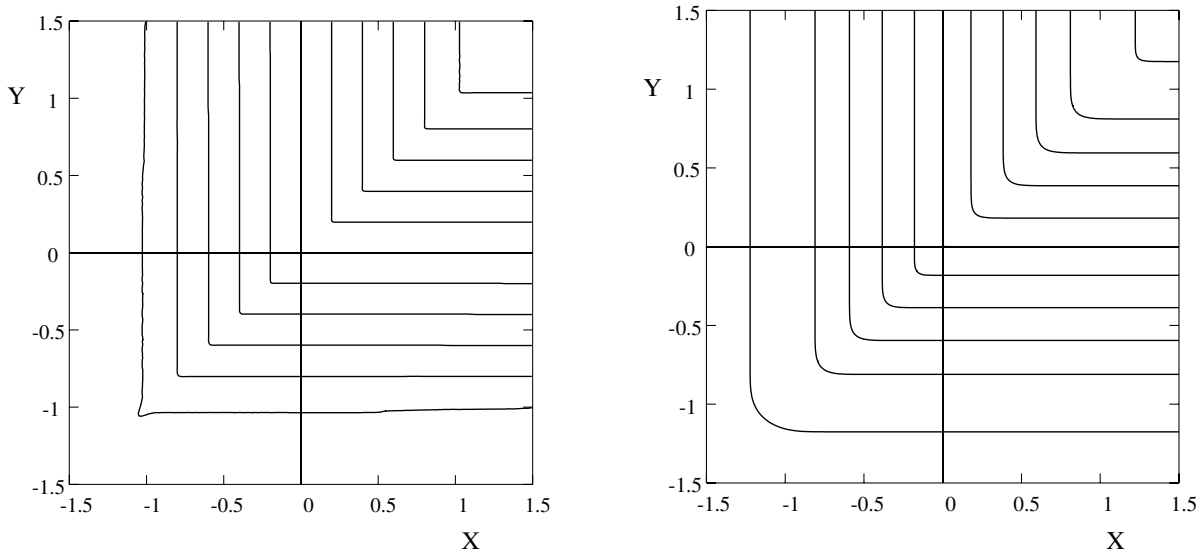

(a) second order integration (GRP) (b) first order integration Godunov)

Fig.5.1: The Burgers equation with initial data (3.1)

In Figures 5 (a)–(b), we display the numerical solutions to the first case (i) of the Burgers equation with initial data (3.1). Comparing the exact solution (3.2) (see Fig. 3.1 (a)) to the numerical solution, we consider separately the "1–D" regions away from the diagonal $x = y$ and the "corner" region near $x = y$. In the "1–D" region, the GRP solution is quite accurate, showing slightly displaced level lines only at the head and tail edges. The Godunov solution, however, shows a much larger "outward" displacement of the head and tail lines. Observe that these are the lines across which the derivative u_x or u_y undergoes a jump discontinuity. The improved resolution of second–order schemes like GRP at such points (even in 1–D computations) is already well established. Turning to the "corner" region near $x = y$, we note that while the GRP solution reproduces quite well the exact pattern of the 2–D rarefaction wave, the Godunov solution is more "rounded" at the corner points, where the x–facing and y–facing rarefaction waves interact. This is a genuinely two–dimensional effect, demonstrating the higher dissipativity of the Godunov scheme.

In Figs.5.2(a) to (b) we display the numerical solutions to the second case (ii) of the Burgers equation with initial data (3.3). Comparing the exact solution (3.4) (see Figure 3.1 (b)) to the numerical solution we see that both schemes reproduce the standing shocks accurately. It demonstrates that this known capability of the Godunov and GRP schemes is unaltered by the two–dimensional splitting.

In Figs.5.3 (a)–(b) we display the numerical solutions to the third case of the Burgers equation, with initial data as in (3.5). Comparing these solutions to the exact solution we see that once again the shocks are well captured by both schemes. Note, however, the sharper resolution of the oblique shock by the GRP scheme.

Finally, in Figures 5 (a)–(b) we display the numerical solutions to the fourth case of the Burgers equation, with initial data (3.6). The exact solution depicted in Figure 3.1 (d) is considerably more complex than in the previous three cases. Note that the sharp wedge at $(-\frac{1}{2}, -\frac{1}{2})$ is "rounded" by both schemes. However, as in the previous cases, the Godunov scheme leads to excessive spreading of the rarefaction wave and the oblique shock (corresponding to parts (I) and (II) of the shock in Figure 3.1 (d)).

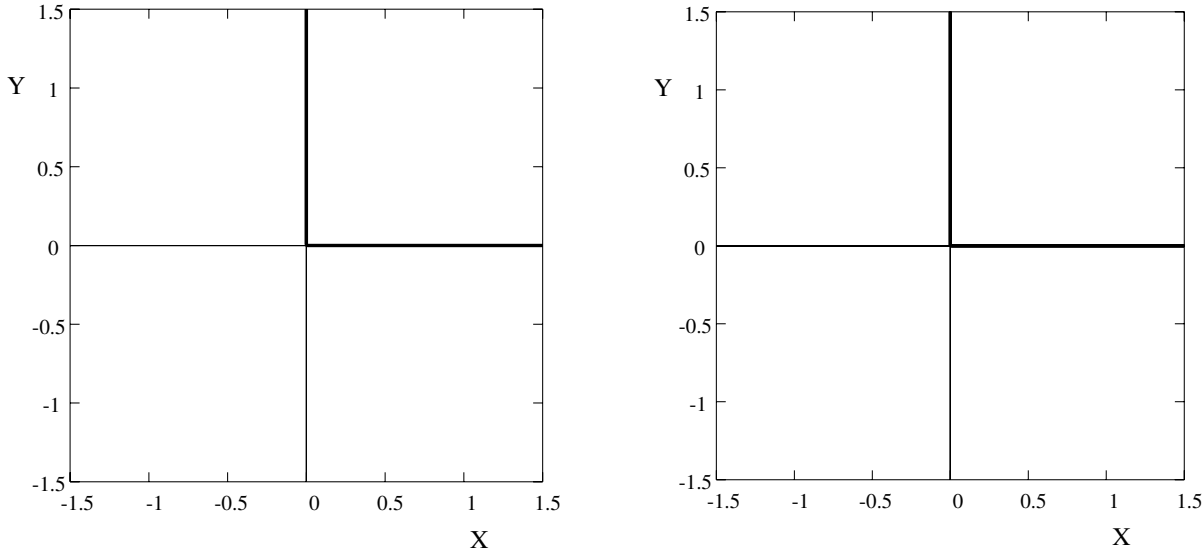

(a) second order integration (GRP) (b) first order integration Godunov)

Fig.5.2: The Burgers equation with initial data (3.3)

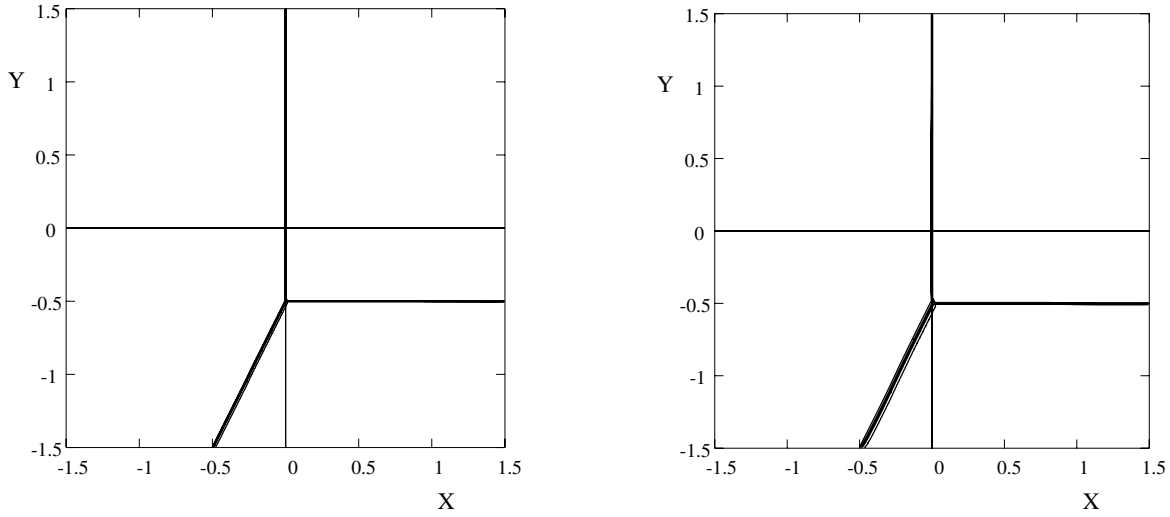

(a) second order integration (GRP) (b) first order integration (Godunov)

Fig.5.3: The Burgers equation with initial data (3.5)

Passing to the Guckenheimer equation with initial data (3.8), we give the numerical results obtained by using both the Godunov and the GRP split schemes. The computation domain was taken to be the square $-1 \le x \le 1$, $-1 \le y \le 1$, which was divided into 320×320 square cells. The time step was $\Delta t = 0.003125$, leading to a CFL number (see (4.18)) $\nu = 0.5$ (since $\max |u| = 1$). The computation was performed up to the final time $t = 1$. The boundary conditions were specified by calculating the exact solution on the outer segments of boundary cells. This is possible as long as the domain boundary is intersected only by the three shocks (a), (b), (c) (see Figure 3.1), which is still true at $t = 1$.

In the following discussion we denote by $U_{i,j}$ the numerical value obtained at time $t = 1$ in cell

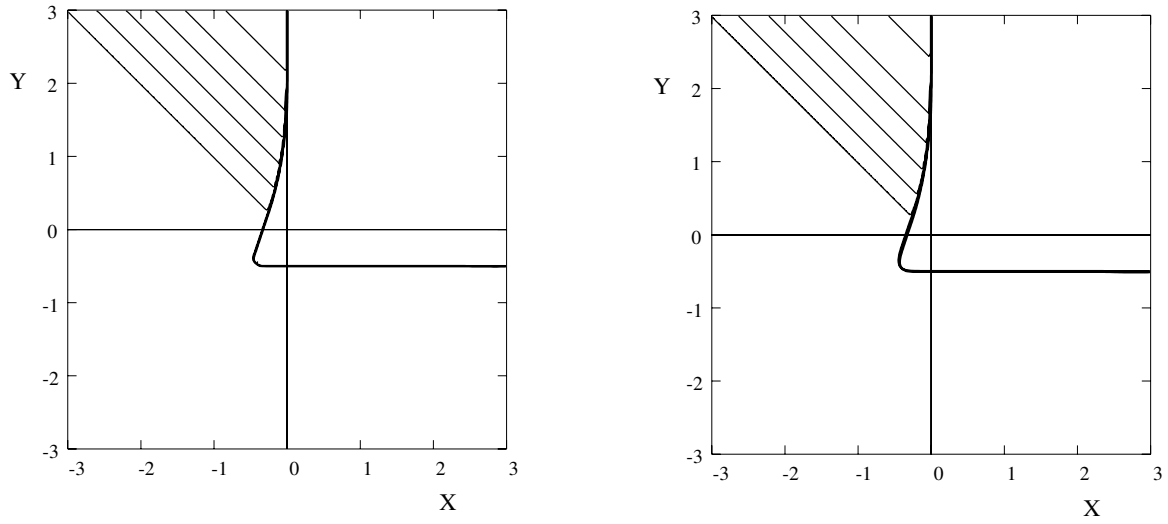

(a) second order integration (GRP) (b) first order integration (Godunov)

Fig.5.4: The Burgers equation with initial data (3.6)

(i,j). The level curves are obtained by interpolating the U values. The results are shown in the sub-domain $[-0.05 \le x \le 0.60,\ 0 \le y \le 0.65]$ (see Fig. 5(a) for the GRP scheme, and Fig. 5(b) for the Godunov scheme). Recall that inside the rarefaction fan $u(x,y,1)$ is constant along the (straight) characteristic lines, so that numerical U-level curves should approximate the fan structure. The U-level sequence (5.1) given below is designed to show the shock fronts and the rarefaction fan. The five levels $L = 9, ..., 13$ correspond to the tail, head and three inner characteristic lines of the rarefaction fan (as shown in Fig.3.3).

$$U_L = \begin{cases} -1 + 0.2\,L & \dots \quad L = 0, 1, ..., 8 \\ 0.60874,\ 0.68295,\ 0.76366,\ 0.86089,\ 1, & \dots \quad L = 9, ..., 13. \end{cases} \tag{5.1}$$

In order to enable interpolation at the lowest and highest U-levels, they were slightly shifted to -0.990 and 0.997, respectively. For comparison of the exact and numerical solutions, we represent the exact solution (Fig. 3.1) by discrete "marker points" situated on shock fronts, as shown in Fig. 5. Additional marker points are located at points (x,y) inside the rarefaction fan, where the exact solution takes on the same values U_L, $L = 9, ..., 13$ as given by (5.1).

Our primary observation with respect to the numerical solution is that both finite–difference schemes, applied according to the operator splitting (4.17), produce a correct approximation to this complex 2–D wave–interaction pattern (see Fig. 5). The GRP solution agrees quite well with the exact one, while the Godunov solution shows a nearly equal agreement for the shock fronts, but a lesser agreement in the rarefaction fan. In this centered fan, the characteristic line that coincides with the sonic shock front corresponds to a constant value of $u = \widetilde{v}$, and it is one of the U-level lines plotted ($L = 9$). In the GRP solution this line is seen very near the sonic shock front (Fig. 5(a)), while in the Godunov case its stand–off distance is perceptibly higher (Fig. 5(b)). The captured sonic shock is represented by the cluster of level lines $L = 0, ..., 9$ (since the jump across this shock is from $u = U_0$ to $u = U_9$). At the other end of the rarefaction fan, the head characteristic line is plotted with $U_{13} = 0.997$ (close to the exact value of $U_{13} = 1$, for a clear U-level interpolation). In the Godunov solution this line extends well beyond the exact solution, while in the GRP solution it agrees well with the exact marker points. The rarefaction fan is the only region of the solution where $u(x,y,1)$

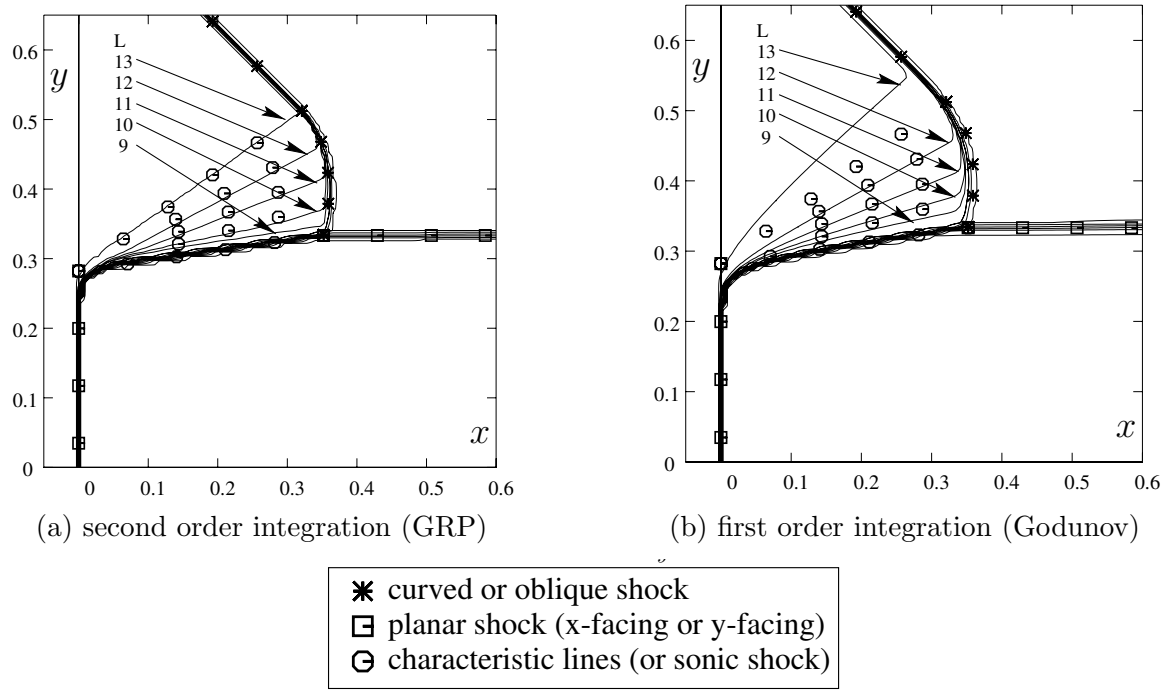

(a) second order integration (GRP) (b) first order integration (Godunov)

Fig.5.5: The Guckenheimer structure both by the GRP and Godunov schemes with coarse grip cells

varies smoothly with a non-zero gradient. Hence, these observations indicate that in such regions the (second–order accurate) GRP scheme produces considerably smaller errors than the (first–order accurate) Godunov scheme. In what concerns the bifurcation point $(0, b)$ and the triple point $(\widetilde{\xi}, \frac{1}{3})$, resulting from the two–dimensional setting, we observe that they are well replicated by both schemes.

Acknowledgements

We are very grateful to Professors Tong Zhang and Peng Zhang for many stimulating discussions concerning the solution to 2-D scalar conservation laws.

Matania Ben-Artzi thanks Beijing Information Technology Institute and the Academia Sinica for the hospitality during his visit in April 2000, when part of this paper was started.

REFERENCES

[1] M. Ben-Artzi and J. Falcovitz: A second-order Godunov-type scheme for compressible fluid dynamics; Journal of Computational Physics, 55:1.32, 1984.

[2] M. Ben-Artzi, J. Falcovitz and U. Feldman: Remarks on high-resolution split schemes computation; SIAM Journal on Scientific Computing, 22:1008.1015, 2000.

[3] S. K. Godunov: A difference scheme for the numerical computation of discontinuous solutions of the equations of fluid dynamics; Mat. Sbornik, 47:271.306, 1959.

[4] J. Guckenheimer: Shocks and rarefactions in two space dimensions; Arch. Rational Mech. Anal., 59:281. 291, 1975.

[5] L. Hörmander: Lectures on Nonlinear Hyperbolic Differential Equations; Springer, New York, 1997.

[6] G. S. Jiang and E. Tadmor: Nonoscillatory central schemes for multidimensional hyperbolic conservation laws; SIAM Journal on Scientific Computing, 19:1892.1917, 1998.

[7] S. Kruzkov: First order quasilinear equations with several space variables; Mat. Sbornik, English Transl. Math USSR-Sbornik, 10:217.243, 1970.

[8] J. Li, S. Yang, and T. Zhang: The Two-Dimensional Riemann Problem in Gasdynamics; Pitman, First edition, 1998.

[9] W. B. Lindquist: Construction of solutions for two-dimensional Riemann problems. Hyperbolic partial differential equations, iii; Comput. Math. Appl. Part A, 12:615.630, 1986.

[10] W. B. Lindquist: The scalar Riemann problem in two spatial dimensions: Piecewise smoothness of solutions and its breakdown; SIAM J. Math. Anal., 17:1178.1197, 1986.

[11] O. A. Oleinik: Uniqueness and a stability of the generalized solutions of the Cauchy problem for a quasilinear equations; USP. Mat. Nauk, Amer. Math. Soc. Transl., Ser. 2, 33:285.290, 1964.

[12] G. Strang: On the construction and comparison of difference schemes; SIAM Journal on Numerical Analysis, 5:506.517, 1968.

[13] A. I. Vol'pert: The space BV and quasilinear equations; Mat. Sbornik, English Transl. Math USSR-Sbornik, 2:225.267, 1967.

[14] D. H. Wagner: The Riemann problem in two space dimensions for a single conservation law; SIAM Journal on Mathematical Analysis, 14:534.559, 1983.

[15] P. Zhang and T. Zhang: Generalized characteristic analysis and Guckenheimer structure; J. Differential Equations, 152:409.430, 1999.

[16] T. Zhang and Y. X. Zheng: Two-dimensional Riemann problem for a single conservation law: Trans. Amer. Math. Soc, 312:589.619, 1989.